



This is a repository copy of *Scattering of massless bosonic fields by Kerr black holes: On-axis incidence*.

White Rose Research Online URL for this paper:
<http://eprints.whiterose.ac.uk/155724/>

Version: Published Version

Article:

Leite, L.C.S., Dolan, S.R. orcid.org/0000-0002-4672-6523 and Crispino, L.C.B. (2019) Scattering of massless bosonic fields by Kerr black holes: On-axis incidence. *Physical Review D*, 100 (8). 084025. ISSN 2470-0010

<https://doi.org/10.1103/physrevd.100.084025>

© 2019 American Physical Society. Reproduced in accordance with the publisher's self-archiving policy.

Reuse

Items deposited in White Rose Research Online are protected by copyright, with all rights reserved unless indicated otherwise. They may be downloaded and/or printed for private study, or other acts as permitted by national copyright laws. The publisher or other rights holders may allow further reproduction and re-use of the full text version. This is indicated by the licence information on the White Rose Research Online record for the item.

Takedown

If you consider content in White Rose Research Online to be in breach of UK law, please notify us by emailing eprints@whiterose.ac.uk including the URL of the record and the reason for the withdrawal request.



eprints@whiterose.ac.uk
<https://eprints.whiterose.ac.uk/>

Scattering of massless bosonic fields by Kerr black holes: On-axis incidence

Luiz C. S. Leite^{1,*}, Sam R. Dolan^{2,†} and Luís C. B. Crispino^{1,‡}

¹*Faculdade de Física, Universidade Federal do Pará, 66075-110, Belém, Pará, Brazil*

²*Consortium for Fundamental Physics, School of Mathematics and Statistics, University of Sheffield, Hicks Building, Hounsfield Road, Sheffield S3 7RH, United Kingdom*



(Received 20 March 2019; published 14 October 2019)

We study the scattering of monochromatic bosonic plane waves impinging upon a rotating black hole, in the special case that the direction of incidence is aligned with the spin axis. We present accurate numerical results for electromagnetic Kerr scattering cross sections for the first time, and give a unified picture of the Kerr scattering for all massless bosonic fields.

DOI: [10.1103/PhysRevD.100.084025](https://doi.org/10.1103/PhysRevD.100.084025)

I. INTRODUCTION

Scattering is a ubiquitous phenomenon in physics across all scales, from particle physics to the cosmic microwave background. The recent observation of “chirps” from binary mergers [1] has shown beyond a reasonable doubt that black holes (BHs) are abundant [2] and that gravitational waves propagate at the speed of light [3]. Of foundational interest, therefore, is the scattering of fundamental fields in the strongly curved spacetime geometry surrounding a BH.

The time-independent scattering of fields by BHs has been studied since the late 1960s, with pioneering early contributions from Matzner and co-workers [4–6], Mashhoon [7], and Sanchez [8]. Recent years have seen advances in calculating accurate scattering cross sections for rotating (Kerr) BHs, overcoming technical difficulties associated with the convergence of the partial-wave series. The massless scalar field ($s = 0$) case was addressed in Ref. [9], and the gravitational wave case ($s = 2$) was given in Ref. [10].

The purpose of this paper is twofold: to present accurate numerical results for the scattering of the electromagnetic field ($s = 1$) by a rotating BH for the first time, and to give a unified description of scattering for all massless boson fields ($s = 0, 1$ and 2), complementing Refs. [11] and [12], for Schwarzschild and Reissner-Nordström scattering, respectively, and Refs. [13] and [14], for Reissner-Nordström and Kerr absorption, respectively.

We consider an idealized scenario, in which a planar wave of frequency ω impinges upon a Kerr BH of mass M and angular momentum $J = aM$ along a direction parallel to its symmetry axis. This scenario is characterized by a pair of dimensionless parameters, $M\omega \equiv GM\omega/c^3$ and

a/M . At low frequency $M\omega \ll 1$, the scattering cross section is [15]

$$\lim_{M\omega \rightarrow 0} \left(\frac{1}{M^2} \frac{d\sigma}{d\Omega} \right) = \frac{\cos^{4s}(\theta/2) + \delta_{s2} \sin^{4s}(\theta/2)}{\sin^4(\theta/2)}, \quad (1)$$

where $\delta_{s2} = 1$ in the gravitational-wave case ($s = 2$) and zero otherwise. Partial polarization is generated at order $O(a\omega)$ by the spin of the BH [10]. The Rutherford-type divergence in the forward direction, of $d\sigma/d\Omega \sim 16M^2/\theta^4$, persists at high frequencies, due to the long-range $1/r$ potential of the Newtonian field. Of greater physical interest is the scattering through large angles, $\theta \gtrsim \pi/2$, which leads to interference effects (orbiting and glories [5,9]) which are a diagnostic of the strong-field region of spacetime that harbors photon orbits, an ergoregion, and the event horizon.

The remainder of this paper is organized as follows. In Sec. II, we briefly review the key equations for linear perturbations in Kerr spacetime. In Sec. III, we provide expressions for the differential scattering cross sections. In Secs. IV and V, we outline the numerical methods and the series reduction method, respectively, used to obtain the results presented in Sec. VI. We conclude with final remarks in Sec. VII. Throughout this paper we use natural units ($G = c = 1$).

II. MASSLESS WAVES ON KERR BACKGROUND

In the Boyer-Lindquist coordinates $\{t, r, \theta, \varphi\}$ the Kerr metric reads

$$ds^2 = -\frac{\Delta}{\Sigma} (dt - a \sin^2 \theta d\varphi)^2 + \frac{\Sigma}{\Delta} dr^2 + \Sigma d\theta^2 + \frac{\sin^2 \theta}{\Sigma} [(r^2 + a^2) d\varphi - a dt]^2, \quad (2)$$

with $\Sigma \equiv r^2 + a^2 \cos^2 \theta$ and $\Delta \equiv r^2 - 2Mr + a^2$. We restrict our attention to the case $a^2 < M^2$, which corresponds to a

*luizcsleite@ufpa.br

†s.dolan@sheffield.ac.uk

‡crispino@ufpa.br

rotating BH with two distinct horizons: an internal (Cauchy) horizon located at $r_- = M - \sqrt{M^2 - a^2}$, and an external (event) horizon at $r_+ = M + \sqrt{M^2 - a^2}$.

On the Kerr background, massless waves are described by the Teukolsky master equation [16], which, when the field $\Upsilon_{\mathfrak{s}}$ is not sourced by any energy distribution, reads

$$\begin{aligned} & \left[\frac{(r^2 + a^2)^2}{\Delta} - a^2 \sin^2 \theta \right] \frac{\partial^2 \Upsilon_{\mathfrak{s}}}{\partial t^2} + \frac{4Mar}{\Delta} \frac{\partial^2 \Upsilon_{\mathfrak{s}}}{\partial t \partial \varphi} \\ & + \left[\frac{a^2}{\Delta} - \frac{1}{\sin^2 \theta} \right] \frac{\partial^2 \Upsilon_{\mathfrak{s}}}{\partial \varphi^2} - \Delta^{-\mathfrak{s}} \frac{\partial}{\partial r} \left(\Delta^{\mathfrak{s}+1} \frac{\partial \Upsilon_{\mathfrak{s}}}{\partial r} \right) \\ & - \frac{1}{\sin \theta} \frac{\partial}{\partial \theta} \left(\sin \theta \frac{\partial \Upsilon_{\mathfrak{s}}}{\partial \theta} \right) + (\mathfrak{s}^2 \cot^2 \theta - \mathfrak{s}) \Upsilon_{\mathfrak{s}} \\ & - 2\mathfrak{s} \left[\frac{a(r-M)}{\Delta} + \frac{i \cos \theta}{\sin^2 \theta} \right] \frac{\partial \Upsilon_{\mathfrak{s}}}{\partial \varphi} \\ & - 2\mathfrak{s} \left[\frac{M(r^2 - a^2)}{\Delta} - r - ia \cos \theta \right] \frac{\partial \Upsilon_{\mathfrak{s}}}{\partial t} = 0, \end{aligned} \quad (3)$$

with \mathfrak{s} being the spin weight of the field, and we have $\mathfrak{s} = 0, \pm 1/2, \pm 1, \pm 3/2, \pm 2$, for scalar, spinorial, electromagnetic, Rarita-Schwinger [17–19], and gravitational perturbations, respectively.

In this paper we focus on bosonic waves; i.e., we choose $\mathfrak{s} = 0, -1$, and -2 , noting the following: for scalar waves $\Upsilon_0 \equiv \Phi$, where Φ is the scalar field; for electromagnetic waves $\Upsilon_{-1} \equiv \phi_2(r - ia \cos \theta)^2$, where $\phi_2 \equiv F_{\mu\nu} \bar{m}^\mu n^\nu$ is a Maxwell scalar, $F_{\mu\nu}$ is the Faraday tensor, and n^μ and \bar{m}^μ are legs of Kinnersley's null tetrad [16]; for

gravitational waves (GWs) $\Upsilon_{-2} \equiv \psi_4(r - ia \cos \theta)^4$, where $\psi_4 = -C_{\alpha\beta\mu\nu} n^\alpha \bar{m}^\beta n^\mu \bar{m}^\nu$ is a Weyl scalar, and $C_{\alpha\beta\mu\nu}$ is the Weyl tensor, which in vacuum coincides with the Riemann tensor.

Using the standard ansatz [16,20–22]

$$\Upsilon_{\mathfrak{s}olm}(t, r, \theta, \varphi) = \mathbf{R}_{\mathfrak{s}olm}(r) \mathbf{S}_{\mathfrak{s}olm}(\theta) e^{-i(\omega t - m\varphi)}, \quad (4)$$

one can separate variables in the master equation [Eq. (3)], obtaining the following pair of differential equations,

$$\left[\left(\Delta \frac{d^2}{dr^2} + (\mathfrak{s} + 1) \Delta' \frac{d}{dr} \right) + \mathbf{V}_{\mathfrak{s}olm}(r) \right] \mathbf{R}_{\mathfrak{s}olm} = 0, \quad (5)$$

$$\left(\frac{d^2}{d\theta^2} + \cot \theta \frac{d}{d\theta} + \mathbf{A}_{\mathfrak{s}olm}(\theta) \right) \mathbf{S}_{\mathfrak{s}olm} = 0, \quad (6)$$

where

$$\mathbf{V}_{\mathfrak{s}olm}(r) \equiv \frac{1}{\Delta} [K^2 - i\mathfrak{s}\Delta'K] - \lambda_{\mathfrak{s}olm} + 4i\mathfrak{s}\omega r, \quad (7)$$

$$\begin{aligned} \mathbf{A}_{\mathfrak{s}olm}(\theta) \equiv & 2a\omega(m - \mathfrak{s} \cos \theta) - \frac{(m + \mathfrak{s} \cos \theta)^2}{\sin^2 \theta} \\ & + \lambda_{\mathfrak{s}olm} + \mathfrak{s} - a^2 \omega^2 \sin^2 \theta, \end{aligned} \quad (8)$$

with $K \equiv (r^2 + a^2)\omega - am$. The angular functions, \mathbf{S} , satisfying Eq. (6) are known in the literature as the spin-weighted spheroidal functions (or harmonics), and the quantities $\lambda_{\mathfrak{s}olm}$ are their eigenvalues. Hereafter, we refer to Eq. (5) as the radial Teukolsky equation (RTE).

TABLE I. Numerical data for the scattering cross section $\frac{d\sigma}{d\Omega}$ for the case $a = 0.99M$, $M|\omega| = 2$. The digits in parentheses give an estimate of the numerical error in the final significant figure quoted, found by comparing $n = 2$ and $n = 3$ iterations of the series reduction method described in Sec. V, with $\ell_{\max} = 60$.

θ	$s = 1$			$s = 2$	
	$s = 0$	$a\omega > 0$	$a\omega < 0$	$a\omega > 0$	$a\omega < 0$
20°	$1.46(3) \times 10^3$	$1.3(8) \times 10^3$	$1.39(8) \times 10^3$	$1.43(8) \times 10^3$	$1.39(8) \times 10^3$
30°	$3.19(1) \times 10^2$	$3.11(4) \times 10^2$	$3.00(5) \times 10^2$	$2.849(8) \times 10^2$	$3.16(2) \times 10^2$
40°	$1.191(1) \times 10^2$	$1.132(3) \times 10^2$	97.1(4)	98.6(4)	$1.251(5) \times 10^2$
50°	46.99(3)	52.67(2)	51.62(5)	62.3(1)	52.14(7)
60°	29.102(2)	23.19(5)	31.836(1)	32.05(2)	21.546(8)
70°	18.829(4)	19.913(2)	14.650(4)	15.163(5)	18.000(2)
80°	7.234(6)	13.37(3)	13.762(7)	15.518(5)	11.361(2)
90°	10.181(1)	7.802(3)	9.775(5)	4.378(2)	4.902(4)
100°	4.9600(3)	10.02(2)	4.5622(4)	9.900(3)	8.884(3)
110°	4.7089(1)	3.3011(1)	8.1650(8)	1.8505(1)	3.6259(1)
120°	6.45237(3)	8.427(2)	2.4888(2)	9.1383(3)	4.5424(4)
130°	1.5715(2)	1.6146(7)	5.5001(1)	1.1628(1)	6.6994(2)
140°	8.6490(4)	8.86690(4)	4.9005(1)	10.5102(1)	1.4553(1)
150°	0.95527(3)	0.8830(3)	2.5716(1)	11.7776(1)	12.34590(7)
160°	12.3040(8)	16.348(1)	12.5921(6)	1.77444(1)	6.6422(1)
170°	9.976(1)	5.1772(3)	7.4316(6)	0.014593(2)	0.09270(5)
180°	77.5562(2)	0	0	$1.1515030(2) \times 10^{-3}$	$2.8316040(5) \times 10^{-4}$

The boundary conditions for the RTE are

$$\mathbb{R}_{\mathfrak{s}\omega lm} \sim \begin{cases} \mathbb{T}_{\mathfrak{s}\omega lm} e^{-i\tilde{\omega}x} \Delta^{-\mathfrak{s}}, & x \rightarrow -\infty, \\ \mathbb{I}_{\mathfrak{s}\omega lm} \frac{e^{-i\omega x}}{r} + \mathbb{R}_{\mathfrak{s}\omega lm} \frac{e^{i\omega x}}{r^{(2\mathfrak{s}+1)}}, & r \rightarrow +\infty, \end{cases} \quad (9)$$

where $\tilde{\omega} \equiv \omega - am/2Mr_+$, and x is the tortoise coordinate in Boyer-Lindquist coordinates, defined by [23]

$$x \equiv r + \frac{1}{r_+ - r_-} [(r_+^2 + a^2) \ln |r - r_+| - (r_-^2 + a^2) \ln |r - r_-|]. \quad (10)$$

III. SCATTERING CROSS SECTION

The differential scattering cross section can be expressed as follows:

$$\frac{d\sigma}{d\Omega} = |\mathfrak{f}(\theta)|^2 + |\mathfrak{g}(\theta)|^2. \quad (11)$$

Using the partial-wave method, the helicity-conserving $\mathfrak{f}(\theta)$ [9,10] and helicity-reversing $\mathfrak{g}(\theta)$ [10] scattering amplitudes can be written as

$$\mathfrak{f}(\theta) = \begin{cases} \frac{2\pi}{i\omega} \sum_{l=0}^{\infty} \mathbf{S}_{0\omega l 0}(0) \mathbf{S}_{0\omega l 0}(\theta) (e^{2i\delta_{0\omega l 0}^{(s=0)}} - 1), & \text{for } s = 0, \\ \frac{2\pi}{i\omega} \sum_{l=1}^{\infty} \mathbf{S}_{-1\omega l 1}(0) \mathbf{S}_{-1\omega l 1}(\theta) (e^{2i\delta_{-1\omega l 1}^{(s=1)}} - 1), & \text{for } s = 1, \\ \frac{\pi}{i\omega} \sum_{P=\pm 1} \sum_{l=2}^{\infty} \mathbf{S}_{-2\omega l 2}(0) \mathbf{S}_{-2\omega l 2}(\theta) (e^{2i\delta_{-2\omega l 2}^{(s=2)}} - 1), & \text{for } s = 2, \end{cases} \quad (12)$$

and

$$\mathfrak{g}(\theta) = \begin{cases} \frac{\pi}{i\omega} \sum_{P=\pm 1} \sum_{l=2}^{\infty} P(-1)^l \mathbf{S}_{-2\omega l 2}(0) \mathbf{S}_{-2\omega l 2}(\pi - \theta) (e^{2i\delta_{-2\omega l 2}^{(s=2)}} - 1), & \text{for } s = 2, \\ 0, & \text{otherwise,} \end{cases} \quad (13)$$

where $e^{2i\delta_{0\omega l 0}^{(s=0)}}$, $e^{2i\delta_{-1\omega l 1}^{(s=1)}}$, and $e^{2i\delta_{-2\omega l 2}^{(s=2)}}$ are the phase shifts which can be computed by integrating the RTE, and θ denotes the scattering angle. We point out that for GWs ($s = 2$) there is a sum over parities ($P = \pm 1$).

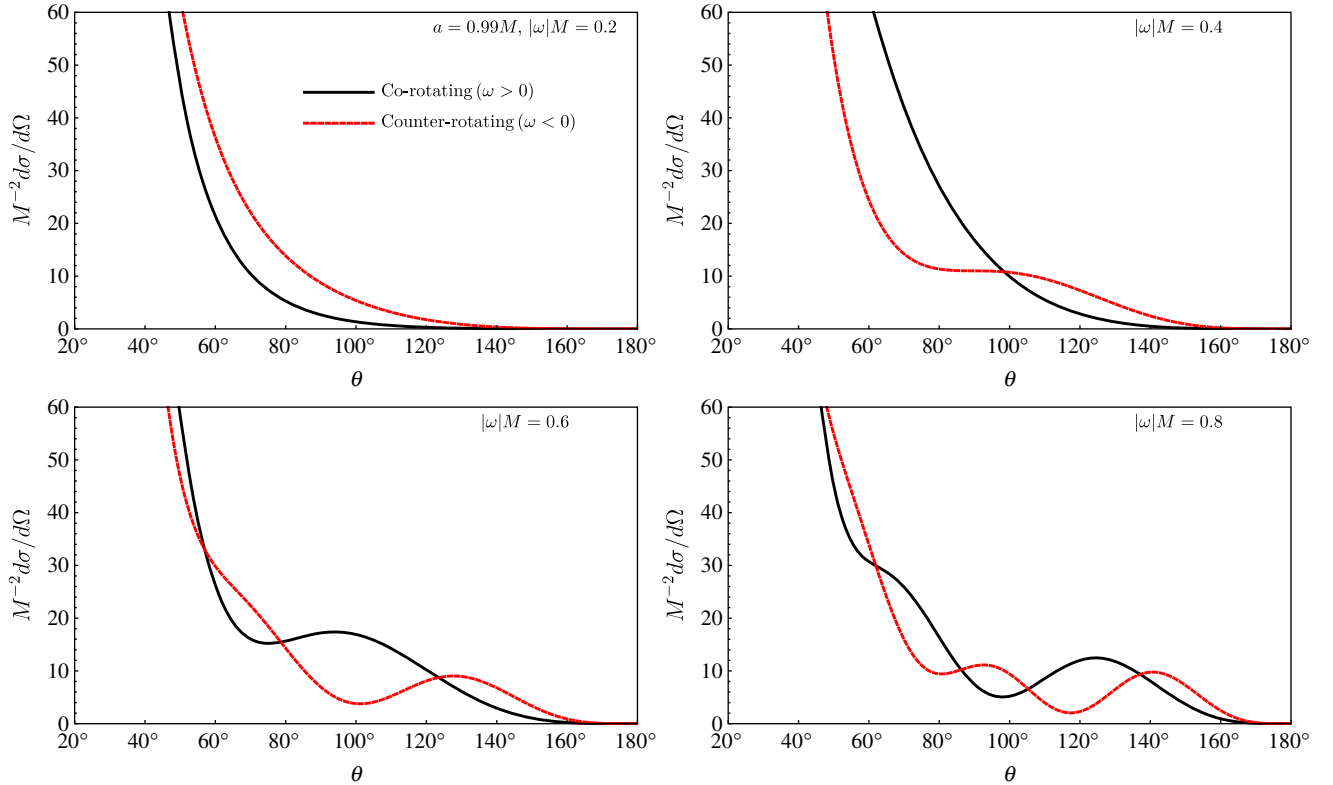


FIG. 1. Low-frequency electromagnetic Kerr scattering cross sections for on-axis incidence. We consider corotating ($\omega M > 0$) and counter-rotating ($\omega M < 0$) polarized electromagnetic waves impinging upon a rapidly rotating ($a = 0.99M$) BH.

The phase shifts are given explicitly by

$$e^{2i\delta_{0\omega l}^{(s=0)}} = (-1)^{l+1} \frac{\mathbb{R}_{0\omega l 0}}{\mathbb{I}_{0\omega l 0}}, \quad (14a)$$

$$e^{2i\delta_{-1\omega l}^{(s=1)}} = (-1)^{l+1} \frac{\mathcal{B}_{\omega l 1} \mathbb{R}_{-1\omega l 1}}{4\omega^2 \mathbb{I}_{-1\omega l 1}}, \quad (14b)$$

$$e^{2i\delta_{-2\omega l 2}^{(s=2)}} = (-1)^{l+1} \left(\frac{\text{Re}(C) + 12i\omega MP}{16\omega^4} \right) \frac{\mathbb{R}_{-2\omega l 2}}{\mathbb{I}_{-2\omega l 2}}, \quad (14c)$$

where $\mathcal{B}_{\omega l 1}^2 = \lambda_{-1\omega l 1}^2 + 4a\omega - 4a^2\omega^2$ and $[\text{Re}(C)]^2 = [(\lambda_{-2\omega l 2} + 2)^2 + 4a\omega - 4a^2\omega^2](\lambda_{-2\omega l 2}^2 + 36a\omega - 36a^2\omega^2) + (2\lambda_{-2\omega l 2} + 3)(96a^2\omega^2 - 48a\omega) - 144a^2\omega^2$. Due to the parity dependence in Eq. (14c), the helicity-reversing amplitude $\mathfrak{g}(\theta)$ is nonzero for GWs [10].

IV. NUMERICAL METHOD

From Eqs. (12) and (13) we note that we need to obtain the spin-weighted spheroidal harmonics (and their eigenvalues) and the phase shifts [Eqs. (14a)–(14c)] in order to use the formula given by Eq. (11). An additional problem impeding the calculation of the scattering cross section is the lack of convergence of the partial-wave series given in Eq. (12).

We obtain the spin-weighted spheroidal harmonics and their eigenvalues via spectral decomposition using the description outlined in Refs. [10,14,24,25], in which

$\mathbb{S}_{\mathfrak{s}\omega lm}$ is written as a sum of spin-weighted spherical harmonics,

$$\mathbb{S}_{\mathfrak{s}\omega jm} = \sum_{l=l_{\min}}^{\infty} b_{\omega j l |\mathfrak{s}|} Y_{\mathfrak{s}lm} \quad (15)$$

where $l_{\min} = \max(|\mathfrak{s}|, |m|)$. In order to obtain the phase shifts, we numerically integrate the RTE using the numerical schemes detailed in Ref. [14].

The long-ranged characteristic of the gravitational interaction leads to a divergence in the amplitude $\mathfrak{f}(\theta)$ at $\theta = 0$ [9,10]. This physical divergence leads to a lack of convergence in the series representation in Eq. (12) for *any* value of θ . In order to improve the convergence properties of the series, we develop and apply a series reduction method, as described in Sec. V.

In a numerical calculation of $d\sigma/d\Omega$, there are several sources of numerical error, including (i) global truncation error in the numerical integration of the RTE; (ii) fitting error in matching the radial solutions to truncated series in the asymptotic regimes ($x \rightarrow \pm\infty$) to obtain phase shifts; (iii) numerical error in application of the series reduction method; (iv) truncation error in terminating an infinite sum at an appropriate l_{\max} . We find that (i) and (ii) are not significant, whereas (iii) and (iv) put a practical limit on the numerical accuracy achieved. For comparison purposes, sample data are given in Table I, along with an error estimate found from the results of applying two and three

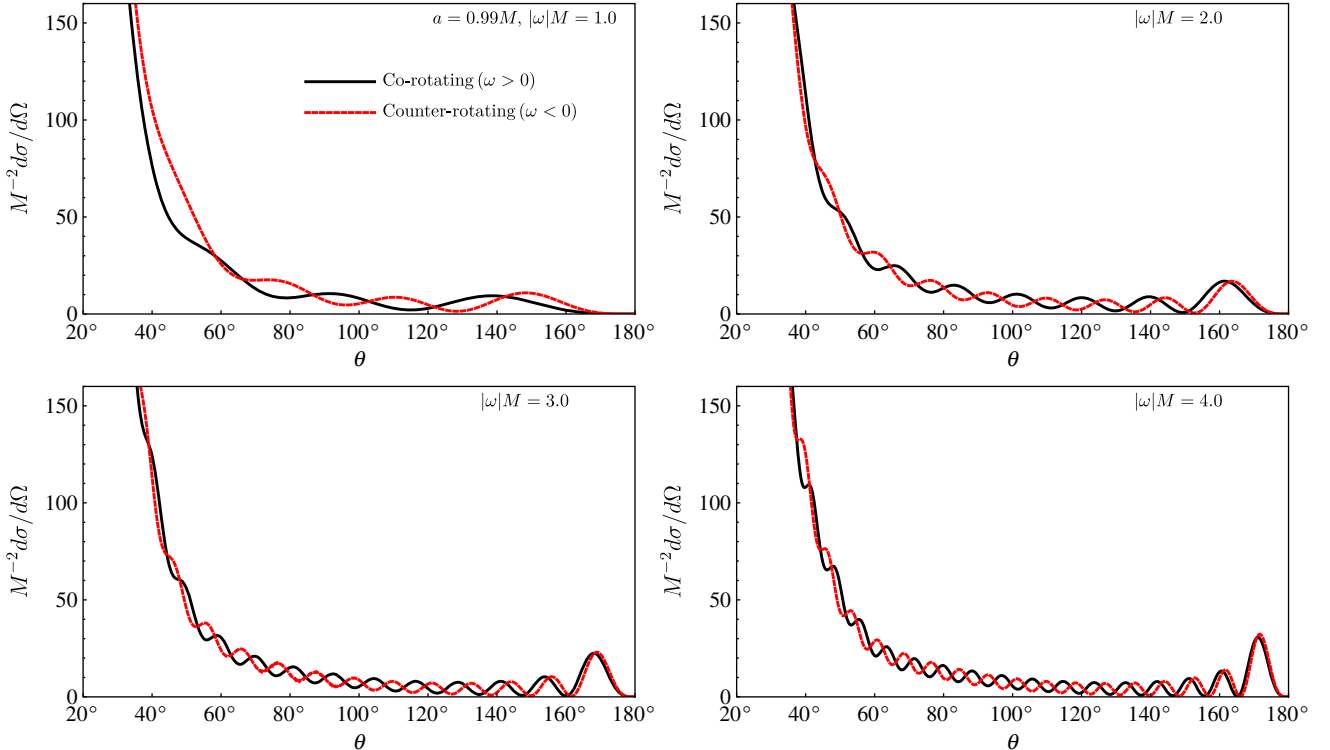


FIG. 2. High-frequency Kerr scattering cross sections for on-axis incidence, showing corotating ($a\omega > 0$) and counter-rotating ($a\omega < 0$) polarized electromagnetic waves impinging upon a rapidly rotating ($a = 0.99M$) BH.

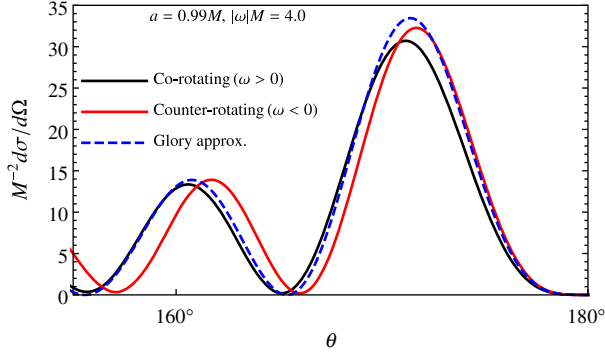


FIG. 3. Electromagnetic scattering for $|\omega|M = 4$ and $a = 0.99M$. The dotted blue line shows the analytical approximation to the glory, Eq. (23), with $s = 1$, $b_g = 5.0925M$, and $db_g/d\theta = -0.2209M$ [10]. The lines show the cross sections of the corotating (black) and counter-rotating (red) polarizations obtained by our numerical method.

iterations of the series reduction method (below) for $l_{\max} = 60$. If required, more precise results could be obtained by increasing l_{\max} .

V. SERIES REDUCTION

The scheme described in this section is inspired by a method developed for numerical computations of

Coulombian scattering [26], which has been successfully employed to compute BHs scattering cross sections [10].

First, let us note that one can rewrite the partial-wave series $\mathbf{f}(\theta)$ [Eq. (12)] and $\mathbf{g}(\theta)$ [Eq. (13)] in the following generic form:

$$F(\theta) = \sum_{l=|\mathfrak{s}|}^{+\infty} F_{l\omega} \mathbf{S}_{\mathfrak{s}l|\mathfrak{s}|}(\theta). \quad (16)$$

Using the spin-weighted spheroidal harmonics spectral decomposition, one can show that the sum over spin-weighted spheroidal harmonics [Eq. (16)] can be rewritten as

$$F(\theta) = \sum_{j=|\mathfrak{s}|}^{+\infty} \mathbb{F}_j Y_{\mathfrak{s}j|\mathfrak{s}|}(\theta), \quad (17)$$

where we have defined $\mathbb{F}_j \equiv \sum_{l=|\mathfrak{s}|}^{+\infty} F_{l\omega} b_{\omega j l|\mathfrak{s}|}$, with $b_{\omega j l|\mathfrak{s}|}$ being the spectral decomposition coefficients of Eq. (15).

The series reduction technique involves defining a new series

$$F(\theta) = (1 - \cos\theta)^{-n} \sum_{j=|\mathfrak{s}|}^{+\infty} \mathbb{F}_j^{(n)} Y_{\mathfrak{s}j|\mathfrak{s}|}(\theta), \quad (18)$$

which has more amenable convergence properties. Noting that $\mathbb{F}_j = \mathbb{F}_j^{(0)}$, the coefficients $\mathbb{F}_j^{(n)}$ can be obtained from the following recurrence relations:

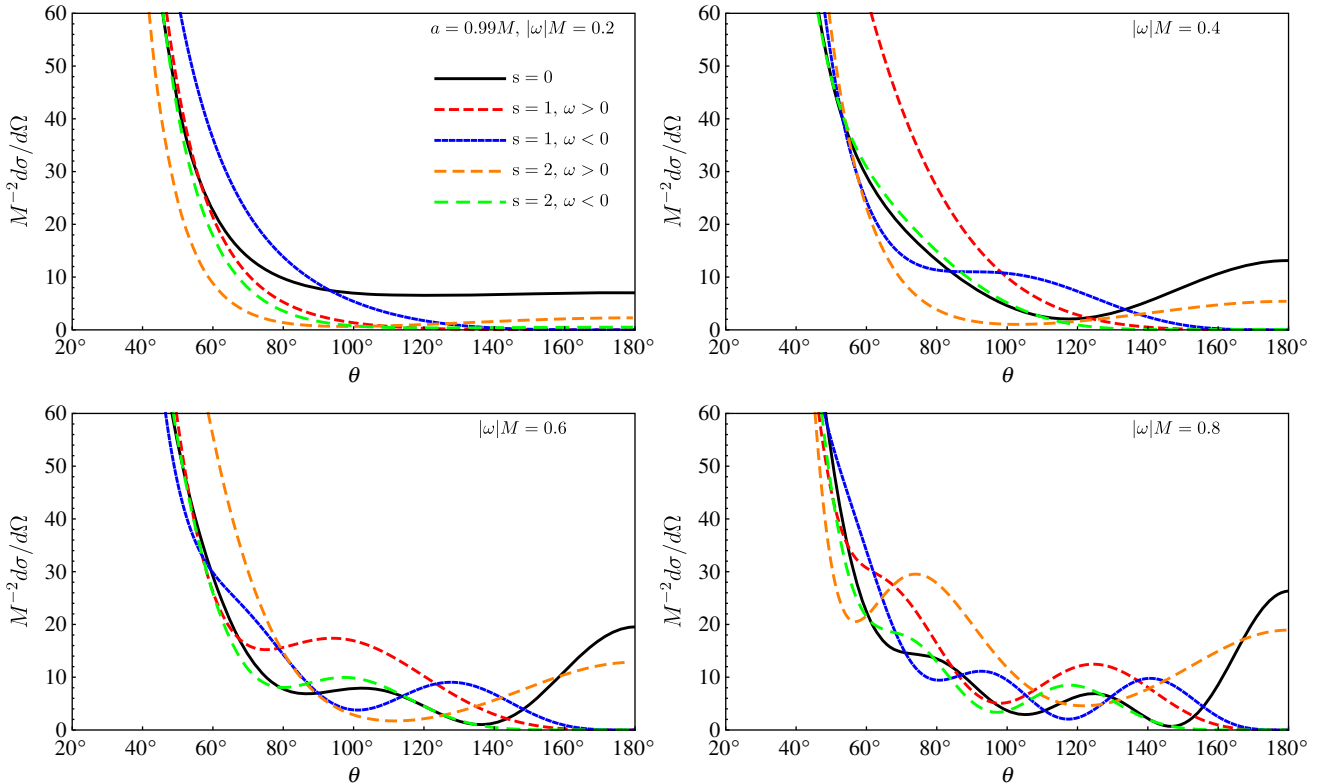


FIG. 4. Long-wavelength ($\omega M < 1$) Kerr scattering cross sections for on-axis incidence, showing both circular polarizations that are corotating ($\omega > 0$) and counter-rotating ($\omega < 0$) with the spin of a rapidly rotating ($a = 0.99M$) BH.

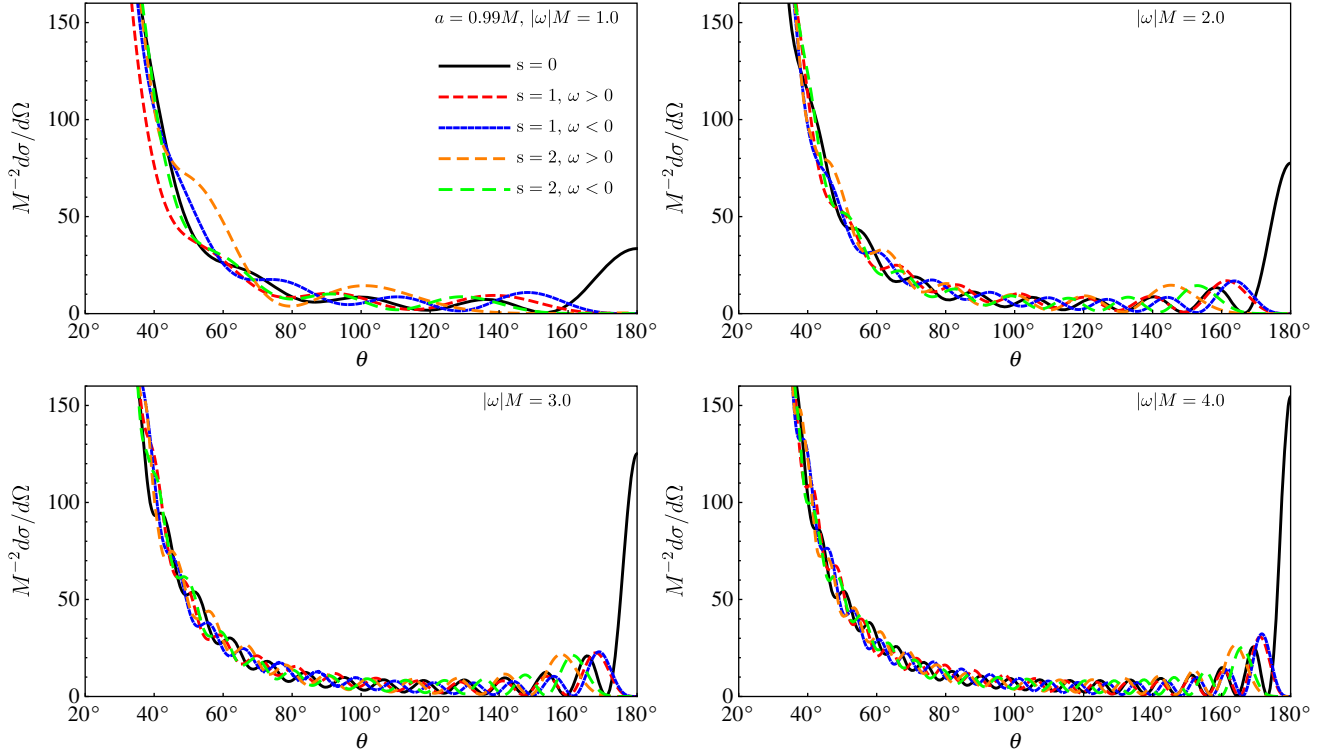


FIG. 5. Short-wavelength ($\omega M \geq 1$) Kerr scattering cross sections for on-axis incidence. We consider scalar ($s = 0$), electromagnetic ($s = 1$), and gravitational ($s = 2$) plane waves impinging on-axis upon a rapidly rotating ($a = 0.99M$) BH.

$$\mathbb{F}_j^{(n+1)} = (1 - \mathcal{X}_{\mathfrak{s}j|\mathfrak{s}|})\mathbb{F}_j^{(n)} - [\mathcal{Y}_{\mathfrak{s}(j-1)|\mathfrak{s}|}\mathbb{F}_{j-1}^{(n)} + \mathcal{Z}_{\mathfrak{s}(j+1)|\mathfrak{s}|}\mathbb{F}_{j+1}^{(n)}], \quad (19)$$

where

$$\mathcal{Y}_{\mathfrak{s}jm} = \sqrt{\frac{(j+1)^2 - m^2}{(2j+1)(2j+3)}} \sqrt{\frac{(j+1)^2 - \mathfrak{s}^2}{(j+1)^2}}, \quad (20)$$

$$\mathcal{Z}_{\mathfrak{s}jm} = \begin{cases} \sqrt{\frac{j^2 - \mathfrak{s}^2}{j^2}} \sqrt{\frac{j^2 - m^2}{4j^2 - 1}}, & \text{for } j \neq 0, \\ 0, & \text{for } j = 0, \end{cases} \quad (21)$$

$$\mathcal{X}_{\mathfrak{s}jm} = \begin{cases} -\frac{m\mathfrak{s}}{j(j+1)}, & \text{for } j \neq 0 \text{ and } \mathfrak{s} \neq 0, \\ 0, & \text{for } j = 0 \text{ or } \mathfrak{s} = 0. \end{cases} \quad (22)$$

The recurrence relations given by Eq. (19) are obtained using the properties of the spin-weighted spherical harmonics. We compute the scattering amplitudes $\mathbb{f}(\theta)$ and $\mathbb{g}(\theta)$ with the help of Eq. (18), with the typical choice of $n = 2$. Moreover, we truncate our series at finite values l_{\max} and j_{\max} , depending on the value of the coupling ωM .

VI. NUMERICAL RESULTS

Figure 1 shows the scattering cross section for low-frequency ($0.2 \leq |\omega|M \leq 0.8$) electromagnetic waves ($s = 1$) impinging upon a rapidly rotating Kerr BH

($a = 0.99M$). Corotating ($a\omega > 0$) and counter-rotating ($a\omega < 0$) waves are scattered in a different way, due to the coupling between the helicity of the field and the rotation of the BH. Thus, a partial polarization is generated in an unpolarized beam by the frame-dragging of spacetime. In the backward direction ($\theta = 180^\circ$), the cross section is zero for both co- and counter-rotating polarizations.

Figure 2 exhibits the scattering cross section for high-frequency electromagnetic waves, demonstrating the existence of orbiting oscillations. The semiclassical interpretation is that these oscillations arise due to constructive or destructive interference between a pair of rays which scatter through θ and $2\pi - \theta$. The angular width of the orbiting oscillation diminishes in inverse proportion to the frequency, as expected. We note that the co- and counter-rotating oscillations have subtly different angular widths.

The cross section in the vicinity of the axis shows a bright spot ($s = 0$) or ring ($s > 0$) known as a glory, which arises from interference between a one-parameter family of rays that originate from an annulus centered on the axis. Matzner *et al.* [5] derived the approximation

$$\frac{d\sigma}{d\Omega} \approx 2\pi M \omega b_g^2 \left| \frac{db}{d\theta} \right|_{\theta=\pi} J_{2s}^2(\omega b_g \sin \theta), \quad (23)$$

where b_g is the impact parameter for the ray scattered through 180° and $J_{2s}(\cdot)$ is a Bessel function. Equation (23)

is valid for any spin s , but it does not distinguish between the co- and counter-rotating polarizations. In Fig. 3 we compare our numerical results with the approximation (23). We see that the two polarizations reach maxima at slightly different scattering angles, with the counter-rotating polarization slightly closer to the axis than the corotating polarization. Although Eq. (23) is a robust approximation, it does not include this effect.

Figures 4 and 5 show the scattering cross sections for massless fields of spin $s = 0, 1$, and 2, corresponding to scalar ($s = 0$), electromagnetic ($s = 1$), and gravitational ($s = 2$) waves impinging along the rotation axis of a rapidly rotating BH ($a = 0.99M$). Figure 4 examines the long-wavelength regime ($0.2 \leq |\omega|M \leq 0.8$). For cases $s > 0$, the cross sections depend on the circular polarization of the wave, with the corotating ($M\omega > 0$) and counter-rotating polarizations ($M\omega < 0$) scattering differently. For EM waves, the cross section is zero in the backward direction ($\theta = 180^\circ$) as the parallel transport of spin leads to destructive interference here. For scalar waves, there is a nonzero backward-scattered flux. For GWs, a nonzero backward flux arises from the helicity-reversing term $|\mathbf{g}|^2$ in Eq. (11). At low frequencies, \mathbf{g} is enhanced for the corotating polarization by superradiance [10].

In Fig. 5, we compare the on-axis Kerr scattering cross sections for short-wavelength ($1.0 \leq |\omega|M \leq 4.0$) massless bosonic waves ($s = 0, 1$, and 2). For $s = 0$, the cross

sections present a glory maximum in the backward direction. For higher-spin waves ($s > 0$), the backward-scattered flux is zero in the electromagnetic case ($s = 1$) and negligible in the gravitational case ($s = 2$) above the superradiance threshold of $\omega > am/(2Mr_+)$ with $m = 2$. The angular width of the spiral scattering oscillations of corotating polarizations are wider than counter-rotating ones, again leading to the generation of a net polarization.

Finally, in Fig. 6 we compare the numerical and analytical [computed through Eq. (1)] results for the on-axis Kerr scattering cross section of long-wavelength waves ($|\omega|M = 0.001$), in the scalar (top panel), electromagnetic (bottom left panel), and gravitational (bottom right panel) cases. We obtain an excellent agreement between the numerical and analytical results.

VII. CONCLUDING REMARKS

We have developed and applied a numerical method to compute the scattering cross section of a Kerr BH for scalar, electromagnetic, and gravitational plane waves, in the special case of on-axis incidence. We found that the scattering cross sections share key features with the static case of spherically symmetric BHs, namely, a forward divergence, spiral scattering oscillations, and a backward glory. A key difference for the Kerr case, however, is that a rotating BH can distinguish between the co- and

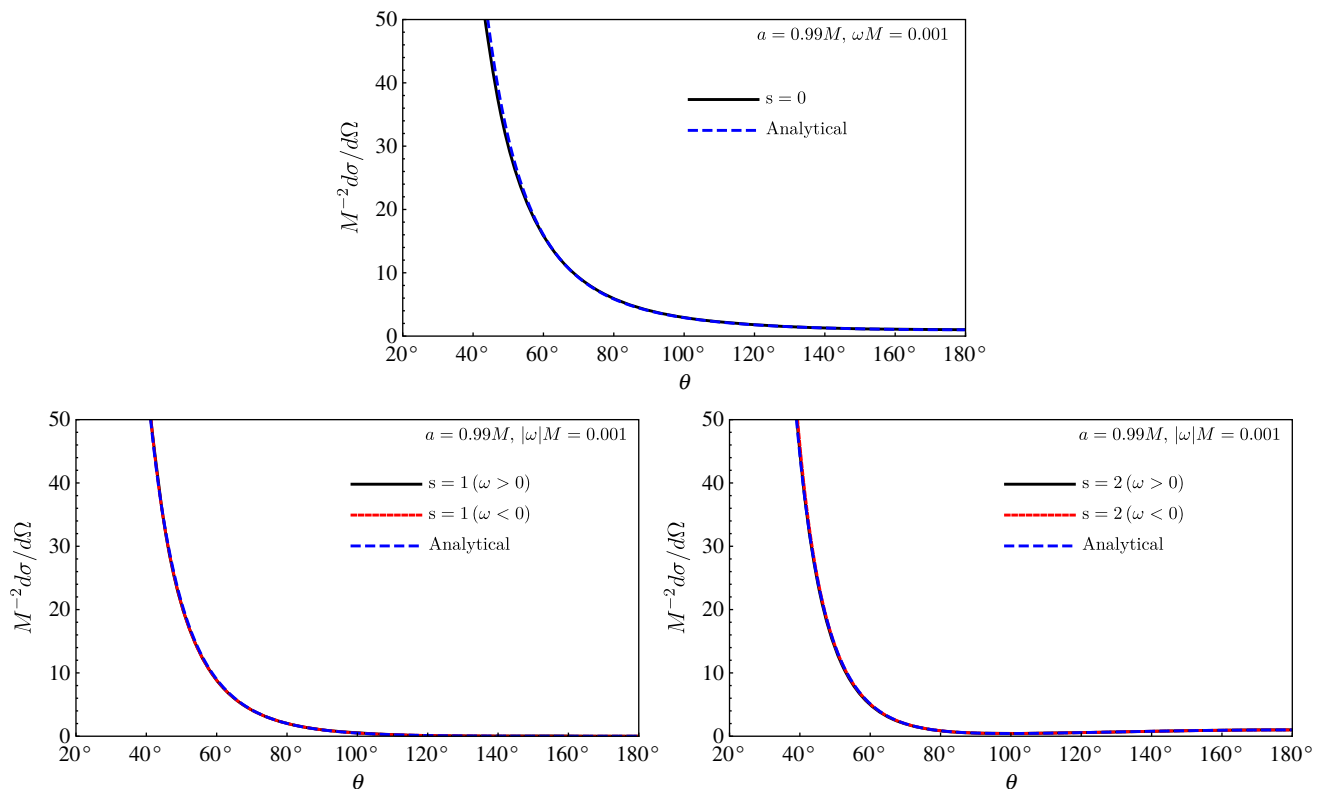


FIG. 6. Comparison between numerical and analytical results for the Kerr scattering cross section in the long-wavelength ($|\omega|M = 0.001$) regime for the case $a = 0.99M$.

counter-rotating circular polarizations of the incident wave [14]. This is a subtle effect that is not accounted for in geometrical optics at leading order.

For nonzero spin waves ($s > 0$), we have shown that a Kerr BH scatters the two polarizations differently, supporting the interpretation of a coupling between the frame-dragging of spacetime and the field helicity. As pointed out in Ref. [10], this coupling has the effect of inducing a partial polarization in an initially unpolarized beam. A consequence of this, manifest in e.g., Figs. 1 and 2, is that the net polarization will vary as one varies the scattering angle.

The semiclassical approximation (23) gives a robust estimate of the glory effect, but it does not account for this coupling between helicity and black hole spin. It seems likely that a more refined approximation could be obtained via the complex angular momentum method; see Sec. IV in Refs. [27] and [28] for results in the Schwarzschild case.

Suppose that one could observe a rotating BH illuminated by broadband radiation at a characteristic frequency of $\omega M \sim 1$. While it is not feasible for a solar-system-based observer to significantly change the observing angle θ , it is feasible to observe the system at several wavelengths. Then, the orbiting phenomenon would lead to regular oscillations in the observed flux with wavelength; and moreover, the frame-dragging of the BH would generate regular oscillations in the polarization state, from predominantly left-handed to predominantly right-handed, and back again.

The results presented here are restricted to the special case of a wave that impinges along the direction of the Kerr rotation axis. In the generic off-axis case, the amplitudes (12) and (13) are found from a double sum, taken over j and m (azimuthal) modes, which is divergent. In Ref. [9], scalar field ($s = 0$) cross sections were calculated by subtracting a Newtonian-type series from this double sum. To treat the higher-spin cases, we propose instead adapting the series reduction method to the off-axis case.

ACKNOWLEDGMENTS

We thank Tom Stratton for helpful comments and discussions. The authors would like to thank Conselho Nacional de Desenvolvimento Científico e Tecnológico (CNPq) and Coordenação de Aperfeiçoamento de Pessoal de Nível Superior (CAPES)—Finance Code 001, from Brazil, for partial financial support. This research has also received funding from the European Union’s Horizon 2020 research and innovation programme under the H2020-MSCA-RISE-2017 Grant No. FunFiCO-777740. L. L. acknowledges the School of Mathematics and Statistics of the University of Sheffield for the kind hospitality while part of this work was undertaken. S. D. acknowledges additional financial support from the Science and Technology Facilities Council (STFC) under Grant No. ST/P000800/1. The authors thank the anonymous referee for valuable comments and suggestions.

-
- [1] B. P. Abbott *et al.* (LIGO Scientific and Virgo Collaborations), Observation of Gravitational Waves from a Binary Black Hole Merger, *Phys. Rev. Lett.* **116**, 061102 (2016).
 - [2] B. P. Abbott *et al.* (LIGO Scientific and Virgo Collaborations), GWTC-1: A Gravitational-Wave Transient Catalog of Compact Binary Mergers Observed by LIGO and Virgo during the First and Second Observing Runs, *Phys. Rev. X* **9**, 031040 (2019).
 - [3] B. P. Abbott *et al.* (LIGO Scientific and Virgo Collaborations), GW170817: Observation of Gravitational Waves from a Binary Neutron Star Inspiral, *Phys. Rev. Lett.* **119**, 161101 (2017).
 - [4] Richard A Matzner, Scattering of massless scalar waves by a Schwarzschild “singularity”, *J. Math. Phys. (N.Y.)* **9**, 163 (1968).
 - [5] R. A. Matzner, C. DeWitte-Morette, B. Nelson, and T.-R. Zhang, Glory scattering by black holes, *Phys. Rev. D* **31**, 1869 (1985).
 - [6] J. A. H. Futterman, F. A. Handler, and R. A. Matzner, *Scattering from Black Holes* (Cambridge University Press, Cambridge, England, 1988).
 - [7] B. Mashhoon, Electromagnetic scattering from a black hole and the glory effect, *Phys. Rev. D* **10**, 1059 (1974).
 - [8] N. G. Sanchez, Elastic scattering of waves by a black hole, *Phys. Rev. D* **18**, 1798 (1978).
 - [9] K. Glampedakis and N. Andersson, Scattering of scalar waves by rotating black holes, *Classical Quantum Gravity* **18**, 1939 (2001).
 - [10] S. R. Dolan, Scattering and absorption of gravitational plane waves by rotating black holes, *Classical Quantum Gravity* **25**, 235002 (2008).
 - [11] L. C. B. Crispino, S. R. Dolan, and E. S. Oliveira, Electromagnetic Wave Scattering by Schwarzschild Black Holes, *Phys. Rev. Lett.* **102**, 231103 (2009).
 - [12] L. C. B. Crispino, S. R. Dolan, A. Higuchi, and E. S. de Oliveira, Scattering from charged black holes and supergravity, *Phys. Rev. D* **92**, 084056 (2015).
 - [13] E. S. Oliveira, L. C. B. Crispino, and A. Higuchi, Equality between gravitational and electromagnetic absorption cross sections of extreme Reissner-Nordström black holes, *Phys. Rev. D* **84**, 084048 (2011).

- [14] L. C. S. Leite, S. R. Dolan, and L. C. B. Crispino, Absorption of electromagnetic and gravitational waves by Kerr black holes, *Phys. Lett. B* **774**, 130 (2017).
- [15] S. R. Dolan, Scattering of long-wavelength gravitational waves, *Phys. Rev. D* **77**, 044004 (2008).
- [16] S. A. Teukolsky, Rotating Black Holes: Separable Wave Equations for Gravitational and Electromagnetic Perturbations, *Phys. Rev. Lett.* **29**, 1114 (1972).
- [17] R. Gueven, Black holes have no superhair, *Phys. Rev. D* **22**, 2327 (1980).
- [18] N. Kamran, Separation of variables for the Rarita-Schwinger equation on all type D vacuum backgrounds, *J. Math. Phys. (N.Y.)* **26**, 1740 (1985).
- [19] G. F. Torres del Castillo and G. Silva-Ortigoza, Rarita-Schwinger fields in the Kerr geometry, *Phys. Rev. D* **42**, 4082 (1990).
- [20] S. A. Teukolsky, Perturbations of a rotating black hole. I. Fundamental equations for gravitational, electromagnetic, and neutrino-field perturbations, *Astrophys. J.* **185**, 635 (1973).
- [21] W. H. Press and S. A. Teukolsky, Perturbations of a rotating black hole. II. Dynamical stability of the Kerr metric, *Astrophys. J.* **185**, 649 (1973).
- [22] S. A. Teukolsky and W. H. Press, Perturbations of a rotating black hole. III-Interaction of the hole with gravitational and electromagnetic radiation, *Astrophys. J.* **193**, 443 (1974).
- [23] A. C. Ottewill and E. Winstanley, The renormalized stress tensor in Kerr space-time: General results, *Phys. Rev. D* **62**, 084018 (2000).
- [24] S. A. Hughes, The evolution of circular, nonequatorial orbits of Kerr black holes due to gravitational wave emission, *Phys. Rev. D* **61**, 084004 (2000); Erratum, *Phys. Rev. D* **90**, 109904(E) (2014).
- [25] G. B. Cook and M. Zalutskiy, Gravitational perturbations of the Kerr geometry: High-accuracy study, *Phys. Rev. D* **90**, 124021 (2014).
- [26] D. R. Yennie, D. G. Ravenhall, and R. N. Wilson, Phase-shift calculation of high-energy electron scattering, *Phys. Rev.* **95**, 500 (1954).
- [27] A. Folacci and M. O. El Hadj, Regge pole description of scattering of scalar and electromagnetic waves by a Schwarzschild black hole, *Phys. Rev. D* **99**, 104079 (2019).
- [28] A. Folacci and M. O. El Hadj, Regge pole description of scattering of gravitational waves by a Schwarzschild black hole, *Phys. Rev. D* **100**, 064009 (2019).